Chemical Science

Accepted Manuscript

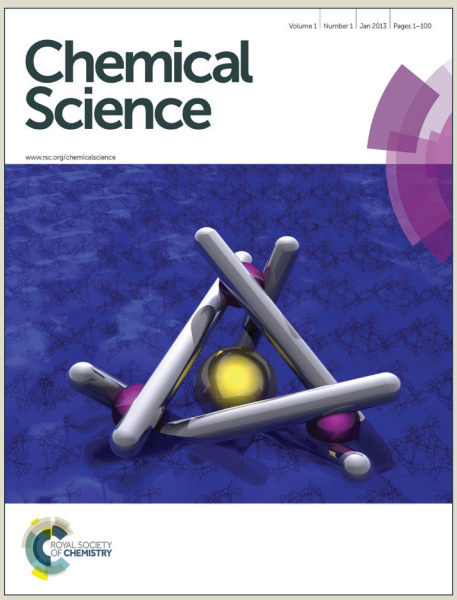

ROYAL SOCIETY OF CHEMISTRY

www.rsc.org/chemicalscience

Journal Name

RSCPublishing

ARTICLE

A Carbon-Carbon Hybrid – Immobilizing Carbon Nanodots and Carbon Nanotubes

Cite this: DOI: 10.1039/x0xx00000x

Volker Strauss[a], Johannes T. Margraf[a,b], Timothy Clark[b], Dirk M. Guldi[a]

Received 00th January 2012,
Accepted 00th January 2012

DOI: 10.1039/x0xx00000x

www.rsc.org/

The thrust of this work is to integrate small and uniformly sized carbon nanodots (CND) with single-walled carbon nanotubes of different diameters as electron acceptors and electron donors, respectively, and to test their synergetic interactions in terms of optoelectronic devices. CNDs (denoted pCNDs, where p indicates pressure) were prepared by pressure-controlled microwave decomposition of citric acid and urea. pCNDs were immobilized on single-walled carbon nanotubes by wrapping the latter with poly(4-vinylbenzyl trimethylamine) (PVBTA), which features positively charged ammonium groups in the backbone. Negatively charged surface groups on the CNDs lead to attractive electrostatic interactions. Ground state interactions between CNDs and SWCNTs were confirmed by a full-fledged photophysical investigation based on steady-state and time-resolved techniques. As a complement charge injection into the SWCNTs upon photoexcitation was investigated by ultra-short time-resolved spectroscopy.

Introduction

Carbon nanomaterials have emerged as important building blocks for a variety of applications that ranges from fiber-reinforced polymer composites to nano-electronic devices.[1–5] This is because they exhibit almost unprecedented potential in terms of structural design and tunable features. Especially in the area of nano-electronics, the opportunities provided by carbon compounds are sheer unlimited.[6-9] Economically and environmentally, carbon nano-materials offer significant advantages over toxic and rare inorganic materials. Despite the enormous progress made in the area of nano-electronics, there is still need for further improvements in, for example, device performance.[10]

The rational synthesis of carbon materials suffers from drawbacks in process-upscaling, reproducibility, and homogeneity.[11] The use of single-walled carbon nanotubes (SWCNT) in, for example, nano-electronics is hindered by a number of factors that include broad structural distributions and lack of solubility. Their functionalization or hybridization by covalent or non-covalent means is essential for making stable SWCNT dispersions. Major breakthroughs in dispersing SWCNTs have been achieved with the help of non-ionic and ionic surfactants, polymer/oligomer wrapping,[12,13] and via non-covalent functionalization with electroactive molecules.[1,14-18]

As a result, some of the newly prepared SWCNT hybrid materials feature superior light harvesting, charge separation or charge transport properties compared to pristine SWCNTs.[19] It is especially important that such a non-covalent approach enables SWCNT optoelectronic devices to be made without perturbing the SWCNT's electronic structure.[20-22] All of these considerations mean that the rational design of hybrid architectures with building blocks designed to perform specific functions is the ultimate goal of many research efforts.[22,23]

In nanoelectronic devices, SWCNT doping by electron donors or acceptors and selective chemical functionalization have proven to be probate means to enhance specific functions of SWCNTs.[14,15,24] For example, in light-harvesting applications, photosensitization with panchromatic light harvesters has shown promise.[23,25-27] Carbon nanodots (CNDs), represent an interesting type of light harvester in this context. They consist of stacked sp^2-hybridized carbon layers with functional groups such as carboxy-, hydoxy-, or amide at the periphery.[7] These nanostructures are known for their tunable light absorption and strong, excitation-dependent photoluminescence. Recently, we demonstrated that CNDs can act as either electron donors or acceptors, depending on their counterpart.[28] All these properties render CNDs ideal candidates for the design of electro- and photoactive hybrids for use in optoelectronic devices.

We now describe the design, synthesis, and characterization of SWCNT/pCND hybrid materials, in which SWCNTs function as charge transporter, and pCNDs (CNDs prepared by pressure-controlled microwave decomposition of citric acid and urea) as charge dopants. The former are known to exhibit extremely high charge carrier mobilities,[29] while the latter have broad absorption cross sections combined with strong fluorescence and with high photostability.[28] A simple and straightforward approach to SWCNT/pCND hybrid materials based on non-covalent hydrophobic and electrostatic forces was selected. First, hydrophobic forces are used to wrap SWCNTs with positively charged poly(4-vinylbenzyl trimethylamine) (PVBTA), as shown in Figure S1. This creates positively charged binding sites at the surfaces of SWCNTs. Electrostatic forces are then used to immobilize negatively charged pCNDs on SWCNTs. The resulting SWCNT/PVBTA and SWCNT/PVBTA/pCND hybrid materials have been fully characterized with particular emphasis on ground- and excited-state interactions between SWCNTs and pCNDs.

Results and Discussion

Characterization of SWCNT/PVBTA hybrids.

PVBTA wrapped SWCNTs have proven to be an ideal platform for immobilizing a variety of nanoparticles.[30,31] Here, the polymer shell functions as a docking site for negatively charged groups of the nanoparticles. In Figure 1, the molecular electrostatic potential (MEP) of an SWCNT/PVBTA model system is shown (see computational details). When in contact, the cationic polymer induces a more positive MEP on the SWCNT.

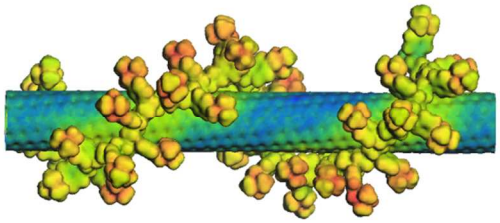

Figure 1. Plot of the molecular electrostatic potential on a 0.03 e^{-} $Å^{-3}$ electron density isosurface of the **SWCNT/PVBTA** system with Cl^{-} counterions. Color scale is from -1830 (blue) to 1950 kcal mol^{-1} (red).

We have used two different types of commercially available SWCNTs, namely CoMoCAT[32] and HiPCO[33] SWCNTs, to probe the influence of SWCNT diameters. Initially, the SWCNT/PVBTA hybrid materials were characterized and compared to sodium dodecylbenzenesulfonate (SDBS) suspended SWCNTs as a SWCNT reference. Here, spectroscopic characterizations by both steady-state and time-resolved absorption and emission spectroscopy together with Raman spectroscopy were complemented by microscopic characterization with transmission electron microscopy (TEM).

In Figure S2, the absorption spectra of HiPCO SWCNT dispersed with the aid of SDBS and PVBTA in D_2O are depicted in black and red, respectively. The red-shifts of the S_{11} transitions in the range from 1050 to 1400 nm are most striking in the PVBTA compared to the SDBS sample. Maxima at 1122, 1176, 1202, 1250, and 1267 nm, which are assigned to (8,4), (12,1), (11,3), (9,5), and (8,7) SWCNTs, respectively, appear red-shifted by 20–30 nm relative to their original positions. An appreciable broadening in the absorption spectra of SWCNT/PVBTA hybrids is evident. Also, the S_{22} transitions in the range between 500 and 800 nm are shifted from, for example, 652 and 735 nm to 658 and 740 nm, respectively. Similar trends in terms of shifting and broadening were published in previous studies.[30,31] Shifts due to differences in background, light scattering, etc. are, however, ruled out.

Likewise, the S_{11} and S_{22} transitions in CoMoCAT SWCNTs shift to longer wavelength (Figure 2) for PVBTA stabilized samples. However, the S_{11} transitions are shifted less than for HiPCO SWCNTs. For example, the (7,5) related S_{11} transition at 1125 nm is shifted by 23 nm to 1148 nm and appears more distinctly pronounced in CoMoCAT SWCNT/PVBTA when compared to the SWCNT/SDBS reference. We conclude that this indicates a high degree of debundling of SWCNTs.[34]

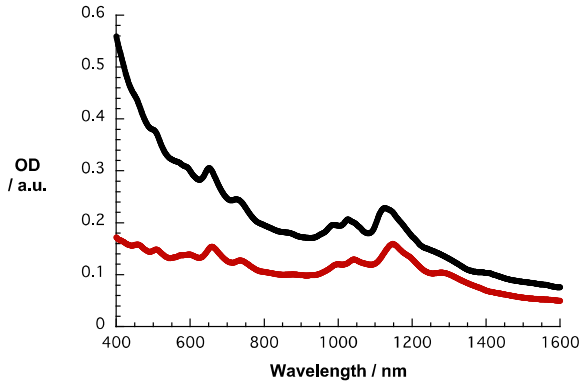

Figure 2. Absorption spectra of **CoMoCAT SWCNT** dispersed with SDBS (2wt%, black) and PVBTA (2wt%, red) in D_2O.

The emission features of SWCNT/PVTBA were also compared with those of SWCNT/SDBS. As a representative example, the the 3D photoluminescence of CoMoCAT SWCNTs dispersed with PVBTA is shown in Figure 3. The corresponding 3D photoluminescence of HiPCO SWCNT in SDBS or PVBTA are shown in Figures S5-S6. At first glance, a striking intensity variation is discernable. Figures 3 and S4-S6 indicate a preferential dispersion of larger diameter SWCNTs within the samples. For CoMoCAT SWCNT/PVBTA the most dominant emission corresponds to that stemming from (7,5) and (7,6) SWCNTs, while for HiPCO SWCNT/PVBTA emission from (7,6), (8,6), and (8,7) prevails. Upon a closer look, red-shifts of the peak positions of at least 25 nm are noticeable – the black cycles in the 3D-PL plot indicate the peak positions of the reference dispersion in SDBS - see also Figures S4-S8. In particular, the (7,5) and (7,6) peaks in CoMoCAT species are shifted from 1036 and 1131 nm to 1059 and 1158 nm, respectively. Likewise, the (9,4), (8,6), and (8,7) peaks in HiPCO samples are shifted from 1109, 1176, and 1265 nm to 1135, 1209, and 1300 nm, respectively. Additional information regarding the quenching of specific SWCNTs present in the samples are given in a statistical analysis in Figure S9. To this end, the strongest quenching was observed for (8,4)-SWCNTs.

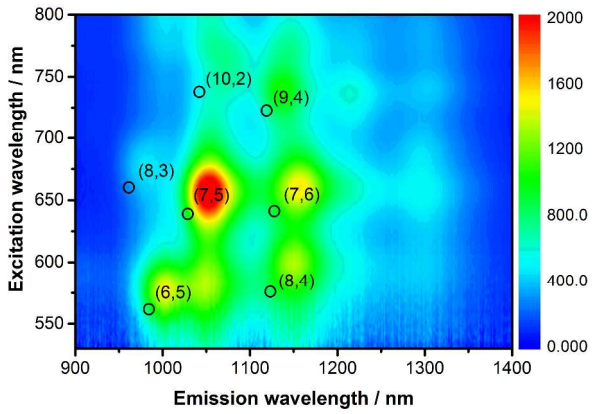

Figure 3. 3D-Photoluminescence plot of **CoMoCAT SWCNT/PVBTA** in D_2O at room temperature. The black circles indicate the positions of the respective features in SWCNT/SDBS in D_2O.

To address selectivity towards specific SWCNTs we conducted Raman experiments, in which we compared SWCNT/SDBS references with SWCNT/PVBTA hybrids, as shown in Figure 4. In the CoMoCAT SWCNT/SDBS reference two radial breathing modes (RBMs) are visible at 266 and 281 cm^{-1}. These are assigned to (7,5) and (7,6) SWCNTs. In CoMoCAT SWCNT/PVBTA only the (7,5) related are detected at 267 cm^{-1}. The lack of (7,6) related RBM is due to the shifting of the resonance energy. Moreover, the comparison of CoMoCAT SWCNT/SDBS and CoMoCAT SWCNT/PVBTA reveals a slight upshift of the G^+-Band. In general, this is interpreted as charge injection into the valence band of SWCNTs.[35] Thus, wrapping with PVBTA moves positive charges close to the SWCNT surface. Complementary experiments with HiPCO samples also imply hole injection, as shown in see Figure S10.

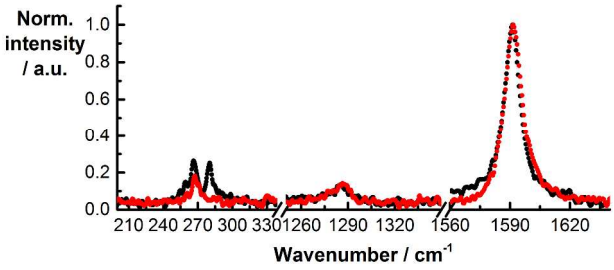

Figure 4: Normalized solid state Raman spectra (λ_{ex} = 1064nm) of **CoMoCAT SWCNT/SDBS** (black) and **CoMoCAT SWCNT/PVBTA** (red) with particular emphasis on the RBM- (left), D-band (center) and G-band (right) regions.

Transmission electron microcopy of CoMoCAT and HiPCO SWCNTs dispersed with PVBTA was used to investigate the quality of the dispersions in terms of homogeneity and individualization. To this end, SWCNT/PVBTA was applied on a Lacey carbon grid and micrographs were taken in different areas of the grid. Representative medium magnification images as shown in Figure S11 the Supporting Information reveal well individualized SWCNTs with lengths of a few hundred nanometers. Notably, only some bundles, each containing a few SWCNTs, were found.

Characterization of SWCNT/PVBTA/pCND hybrids.

Initial investigations of the interactions between SWCNT/PVBTA and pCND aimed at absorption titration assays, in which the SWCNT/PVBTA concentrations were kept constant and variable concentrations of pCND were added stepwise. Here, SWCNT/PVBTA suspensions with optical densities of approximately 0.2 at a given reference point were used – see Experimental Section for details. Figure 5 shows a sequence of absorption spectra of CoMoCAT SWCNT/PVBTA in the presence of increasing pCND concentrations – with absorptions in the 300 to 400 nm range – from black to red. The large shifts of the S_{11} transitions in the near infrared are striking. For example, (6,5), (7,5), and (8,4) related peaks reveal 12 to 15 nm shifts from 1045, 1152, and 1281 nm to 1058, 1164, and 1296 nm, respectively. Even the S_{22} absorption bands of (7,5)/(7,6) and (8,7) are noticeably shifted from, for example, 660 and 736 nm to 663 and 740 nm, respectively. Considering the aforementioned changes in concert and the fact that SWCNT/PVBTA were kept constant, we infer a substantial shift of charge density between SWCNTs and pCNDs.

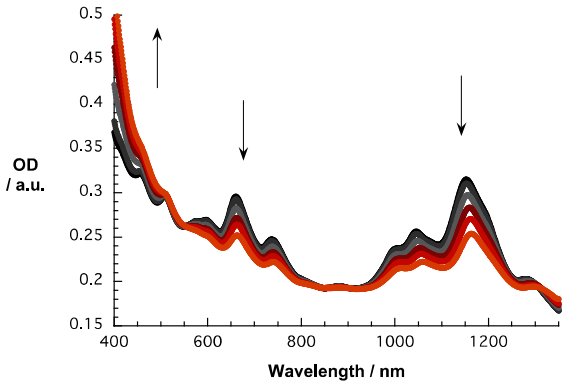

Figure 5. Absorption spectra recorded in the course of sequential addition of **pCND** to **CoMoCAT SWCNT/PVBTA** in D_2O at room temperature – arrows refer to the course of addition.

Absorption titrations of HiPCO SWCNT/PVBTA with pCNDs reveal qualitatively similar trends. Figure S12 shows the absorption spectra of HiPCO SWCNT/PVBTA and SWCNT/PVBTA/pCND in black and red, respectively. Several maxima in the near-infrared region, for example, at 1149, 1196, 1286 nm, undergo shifts of approximately 15 nm to the red side of the spectrum. Here, diminishing S_{11} transitions throughout the titrations indicate strong electronic coupling between pCNDs and HiPCO SWCNTs.

As a complement to the absorption titrations, we used the same suspensions and conducted near-infrared emission measurements to monitor changes in the SWCNT centered emission. As an example, the emission spectra of pure

CoMoCAT SWCNT/PVBTA in D_2O and with increasing concentrations of pCNDs excited at 650 nm are shown in Figure 6. The maxima at 1058, 1158, and 1295 nm resemble the electronic S_{11} transitions of (7,5), (7,6), and (9,5) SWCNTs. Notably, addition of pCNDs leads to quantitative but also unselective quenching of the emission. A 15 to 20 nm red shift evolves during the quenching; a trend that is in sound agreement with what is seen in the absorption titrations. In particular, the aforementioned peaks now appear at 1073, 1177, and 1315 nm. The corresponding 3D-photoluminescence plots are shown in Figure S14. Similar observations were obtained in complementary experiments with HiPCO SWCNTs – Figures S15 and S16.

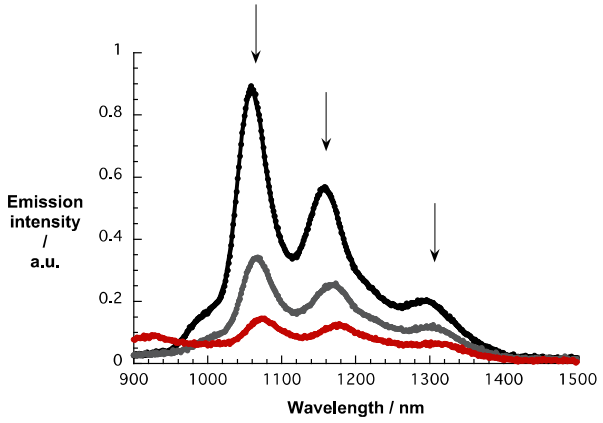

Figure 6. NIR emission spectra of **CoMoCAT SWCNT/PVBTA** upon excitation at 650 nm recorded during sequential addition of **pCND** in D_2O at room temperature – arrows refer to the course of addition,

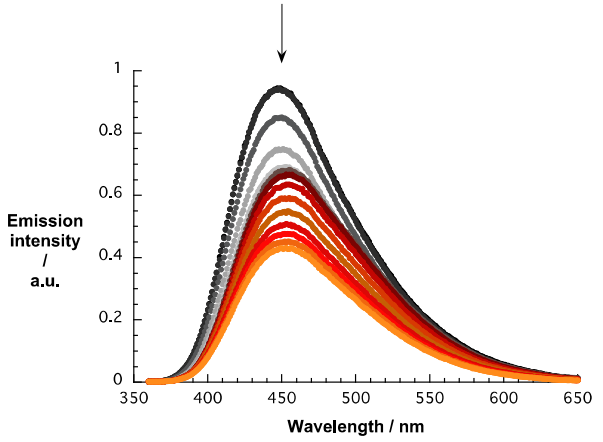

Figure 7: Emission spectra of pCND during the course of a titration with **CoMoCAT SWCNT/PVBTA** in D_2O at room temperature – arrow refers to the course of addition.

To verify these observations, we performed reversed titration experiments, in which we started with a given pCND concentration and added CoMoCAT SWCNT/PVBTA sequentially. In this case, a gradual increase of the SWCNT-related transitions was observed accompanied by a noticeable blue shift during the titration – Figure S13.

The quenching of the pCND emission in the range around 450 nm during the reverse titrations gives rise to several interesting effects. Overall, the emission shifts from 446 to 458 and back to 453 nm, as shown in Figure 7. A more profound analysis of the emission evolution was performed by fitting the spectra with an asymmetric double sigmoidal function.

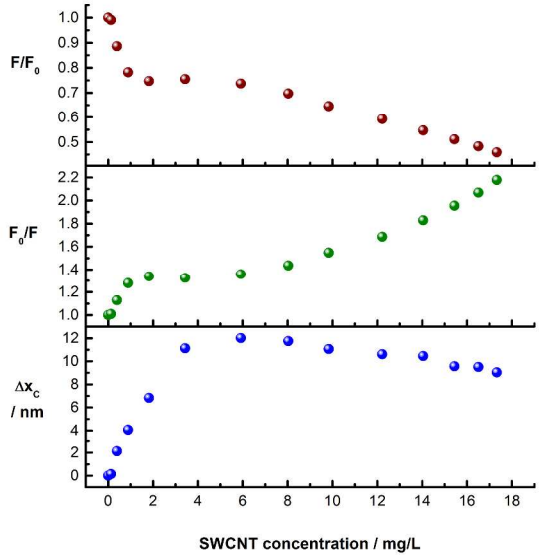

Figure 8. Evolution of the emission spectra of **pCND** in dependence of the amount of **CoMoCAT SWCNT/PVBTA** added in D_2O at room temperature. Upper panel (F/F_0) Quenching of the emission intensity. Center panel (F_0/F): Corresponding Stern-Volmer plot. Lower panel (x_C): Shift of the peak maximum.

The evolution of the pCND related emission during the course of the titration with CoMoCAT SWCNT/PVBTA is shown in Figure 8. The upper and the central plots show the quenching (F/F_0 and F_0/F) plotted against SWCNT/PVBTA concentration. Strong quenching is observed up to a SWCNT/PVBTA equivalent of 2 mg/L, followed by a plateau up to concentrations of 6 mg/L. Upon further addition, more fluorescence quenching at a different rate sets in. Interestingly, this quenching correlates well with the shift of the maximum. The lower plot in Figure 8 shows the evolution of the peak location versus SWCNT/PVBTA concentration. Again, a strong red-shift of 12 nm (from 446 to 458 nm) was observed in the concentration range between 0 and 4 mg/L. This shift is replaced by a weaker blue shift from concentrations of 8 mg/L onwards.

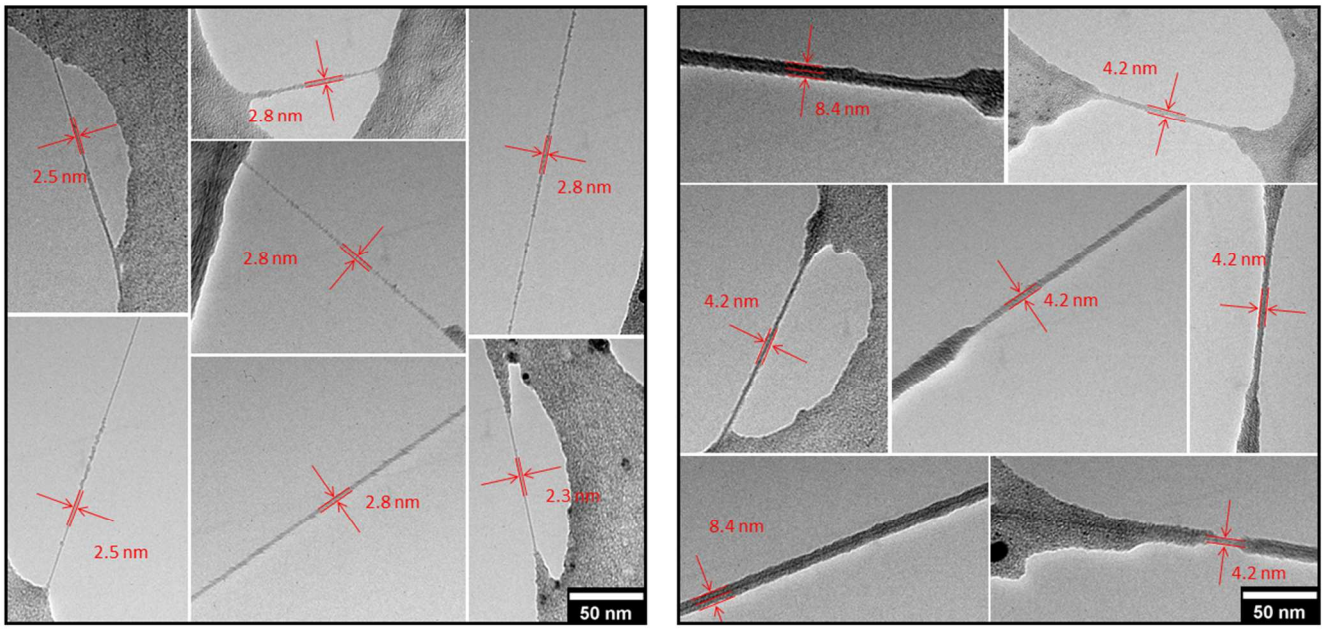

Figure 10. Representative TEM images of freestanding **CoMoCAT SWCNT/PVBTA** (left) and **CoMoCAT SWCNT/PVBTA/pCND** (right) on a Lacey carbon support film.

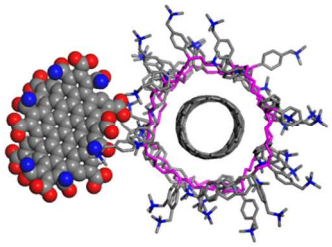

Figure 9. Structure of a **SWCNT/PVBTA/pCND** hybrid extracted from a molecular dynamics simulation.

These experiments clearly prove the interactions between both components. To obtain a qualitative structural model of the hybrid system, we performed molecular dynamics (MD) simulations (see computational details). Figure 9 shows one structure of a SWCNT/PVBTA/pCND model system, taken from a molecular-dynamics (MD) simulation. The negatively charged pCND interacts with the cationic polymer to form the hybrid material in solution. These simulations indicate that the observed electronic communication is not due to π-π-interactions.

Transmission electron microscopic analyses of SWCNT/PVBTA after immobilization of pCND reveal individualized SWCNT/PVBTA/pCND throughout the entire TEM grid. Images documenting the individualization are shown in Figure S17. The diameters of SWCNT wrapped with PVBTA are expected to be in a range between 2 – 3.5 nm, while those of the SWCNT/PVBTA/pCND assemblies should feature diameter between 4 and 5 nm. These diameters are in sound agreement with our TEM investigations. Both SWCNT/PVBTA and SWCNT/PVBTA/pCND were applied on Lacey carbon film supported TEM grids to obtain freestanding SWCNTs. As aforementioned, drying of the samples leads to the formation of a thin polymer films, into which the SWCNT assemblies are incorporated. The TEM images in Figure 10 show a series of micrographs of individual SWCNT/PVBTA (upper part) and SWCNT/PVBTA/pCND (lower part). From the latter diameters of 2.3 – 2.8 nm for SWCNT/PVBTA and ~4.2 nm or ~8.4 nm for individualized SWCNT/PVBTA/pCND and smaller bundles thereof, respectively, were determined.

Next, we probed the effect of addition of SWCNT/PVBTA on the emission lifetimes of pCND. Overall, the decays obtained by time-correlated single-photon counting (TCSPC), which spanned through a few tens of ns, were best fit by triexponential functions to obtain χ^2 values with standard errors less than 1 ± 0.01 to yield lifetimes of 2, 6, and 12 ns. Upon addition of SWCNT/PVBTA, all three lifetimes are reduced significantly, as shown in Table 1. Strikingly, the shortest lifetime begins to dominate when SWCNT/PVBTA is present. Lifetime measurements conducted with CoMoCAT and HiPCO SWCNT/PVBTA reveal similar trends – Figures S18 and S19.

Table 1. Emission lifetimes and their corresponding amplitudes obtained by TCSPC for pCND with different amounts of CoMoCAT SWCNT/PVBTA. Samples were excited at 403 nm and time profiles were fitted at 445 nm.

	τ_1 [ns]		τ_2 [ns]		τ_3 [ns]	
pCND	2.0	(26%)	6.0	(38%)	12	(36%)
pCND/SWCNT/ PVBTA(1)	0.4	(49%)	2.4	(26%)	9.1	(24%)
pCND/SWCNT/ PVBTA(2)	0.4	(48%)	2.4	(28%)	7.5	(24%)

To gain deeper insight into doping of SWCNTs on addition of pCND, we conducted complementary Raman experiments with

SWCNT/PVBTA and SWCNT/PVBTA/pCND. The G^+-band, as well as the 2D-band, show appreciable down-shifts upon adding pCND to both CoMoCAT and HiPCO SWCNT/PVBTA, suggesting that electrons are donated from pCNDs to SWCNTs – Figure 11 and S20. The observed G-band shift of 2.3 cm^{-1} from 1594.2 to 1591.9 cm^{-1} in the case of cSWCNT is very large for chemical doping of SWCNTs.[35]

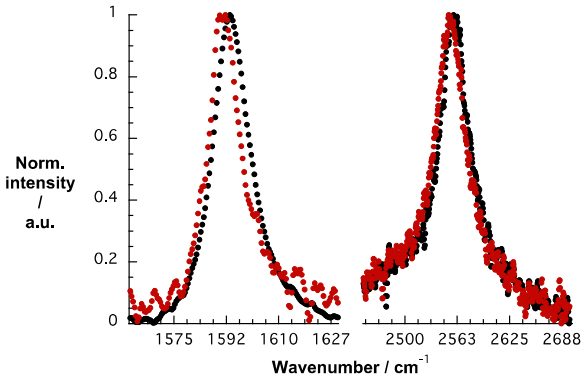

Figure 11. Normalized solid state Raman spectra (λ_{ex} = 1064nm) of **CoMoCAT SWCNT/PVBTA** (black) and **CoMoCAT SWCNT/PVBTA/pCND** (red) with particular emphasis on the G-band and 2D-region.

We turned to femtosecond transient absorption spectroscopy to investigate the charge-transfer dynamics. Here, the excited state dynamics of SWCNT/PVBTA were investigated and compared with those of SWCNT/PVBTA/pCND. All samples were excited at 387 nm, where both pCND and SWCNT feature appreciable ground state absorptions, or at 660 nm, where SWCNT are selectively excited. Immediately upon photoexcitation of CoMoCAT SWCNT/PVBTA, a set of transient maxima at 1255, and 1364 nm and minima at 997, 1048, 1152 and 1287 nm evolve, as shown in Figure 12. These represent the excited-state features of CoMoCAT SWCNTs.[16] The bleaching features in the NIR are reflections of the ground state bands, seen in the absorption experiments. The ground state recovery of CoMoCAT SWCNT/PVBTA takes place within a few hundred picoseconds and is characterized by three different lifetimes: 2, 25, and 260 ps.

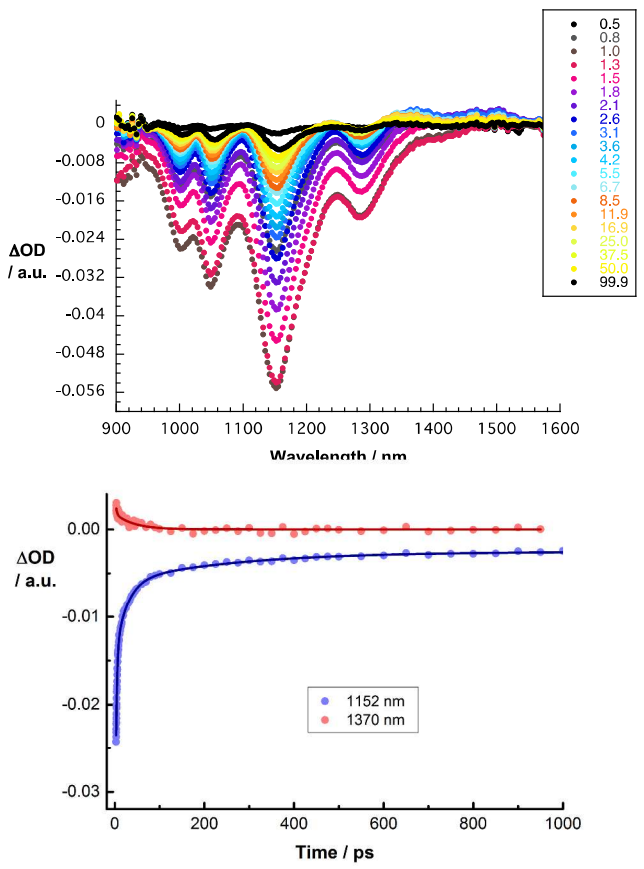

Figure 12. Upper part – differential absorption spectra obtained upon femtosecond pump probe experiments (λ_{ex} = 387 nm) of **CoMoCAT SWCNT/PVBTA** with several time delays between 0.5 and 99.9 ps at room temperature. Lower part – corresponding time absorption profiles of the spectra shown left at 1150 nm (black) and 1400 nm (red) monitoring the excited state decay.

Several conclusions can be drawn from the transient absorption spectra of CoMoCAT SWCNT/PVBTA/pCND. In particular, an overall red shift of the aforementioned maxima to 1255 and 1370 nm and minima to 1010, 1059 and 1161 and 1298 nm is observed in the initial spectrum, as shown in Figure 13. Relative to CoMoCAT SWCNT/PVBTA, this reflects the formation of a complex between CoMoCAT SWCNT/PVBTA and pCND, in which a substantial delocalization of charge density shifts the SWCNT centered bleaching to lower energies – *vide supra*. As time progresses, the dominant minima, which correspond to the ground state bleaching in the NIR, shift to, for example, 1014, 1065 to 1166 and 1294 nm. In addition, the 1255 nm maximum, appears with an additional lifetime component. Considering that all of these features are assigned to reduced CoMoCAT SWCNTs – as established in previous work based on complementary spectroelectrochemical and photophysical assays[25] – we infer the formation of a charge separated state. In the context of oxidized pCND, we turned to its electrochemical oxidation as shown in Figures S21 and S22 in the Supporting Information. To this end, upon oxidation the ground state absorption at around 350 nm decreases in

intensity, while new absorption features between 400 – 600 nm are noted. In the transient absorption spectra this spectral region is, however, dominated by SWCNT centered absorptions.[36] The correspondingly formed reduced CoMoCAT SWCNTs and oxidized pCNDs recombine with a lifetime of 105 ± 11 ps.[20] The lifetimes for HiPCO SWCNT/PVBTA/pCND – Figure S24 – are 20 ± 5 ps for the charge separated state lifetime.

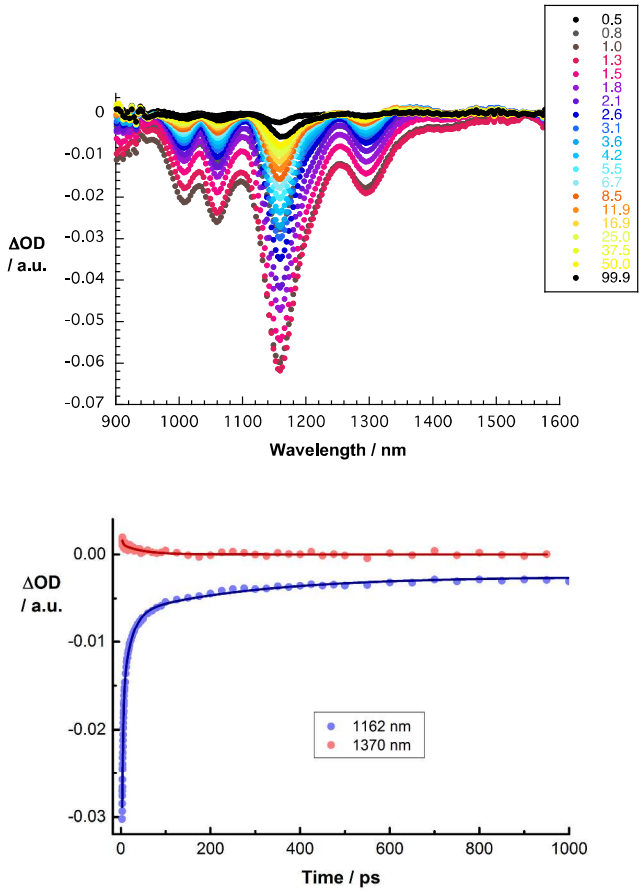

Figure 13. Upper part – differential absorption spectra obtained upon femtosecond pump probe experiments (λ_{ex} = 387 nm) of **CoMoCAT SWCNT/PVBTA/pCND** with several time delays between 0.5 and 99.9 ps at room temperature. Lower part – corresponding time absorption profiles of the spectra shown left at 1150 nm (black) and 1400 nm (red) monitoring the excited state decay.

Conclusions

In summary, we have successfully decorated SWCNTs with pCNDs. The pCNDs used in this work are rather monodisperse with very large bandgaps on the order of 3.2 eV (Figure S3) and served as electron donors. Immobilization of the negatively charged pCNDs onto SWCNTs was enabled by means of wrapping with a positively charged polymer, namely PVBTA.

The herein presented results all suggest effective charge transfer between SWCNTs and pCNDs in the ground and excited state. First evidence came from steady state absorption and emission titrations. Upon addition of pCND to the SWCNT/PVBTA hybrid, appreciable red shifts and decrease of the SWCNT-related absorption features were observed. These coincided with a noticeable quenching and shifting of the pCND and SWCNT related emission. Shifted pCND and SWCNT absorptions / emissions point to a redistribution of charge density, that is, from pCNDs to SWCNTs. Further corroboration for this hypothesis came from rather strong downshifts of the G-band in Raman experiments with SWCNT/PVBTA and SWCNT/PVBTA/pCND. Full charge separation, that is, formation of a charge separated state with reduced CoMoCAT SWCNTs and oxidized pCNDs was found in pump probe experiments.

Experimental Section

The preparation of pressure Carbon Nanodots (pCND) has been described previously.[28] CoMoCAT SWCNTs SG 76, enriched with (7,6) SWCNTs were obtained from Sigma Aldrich. HiPCO SWCNTs super-purified were obtained from Unidym.

SWCNT/PVBTA hybrids were prepared by mixing 0.1 mg SWCNT and 1 mg PVBTA in 5 mL D_2O. The mixture was sonicated using bath-type sonication at (37 kHz, Power: 100%) at room temperature for 30 min and then centrifuged at 15 kG for 10 min. The supernatant liquid was used for spectroscopic analysis. For the spectrophotometric titrations SWCNT suspensions with optical densities of ~0.2 at 850 and 950 nm for CoMoCAT and HiPCO, respectively, were prepared. The SWCNT suspensions were divided in two portions. To one portion solid pCND was added to obtain a concentration of 20 mg L^{-1}. For the titrations the pCND containing portion was added stepwise to the pure SWCNT/PVBTA suspension.

Ultrasonication used for the preparation of SWCNT suspensions was carried out with a Elmasonic P120 52 (330 W) from ELMA. Steady-state absorption measurements were carried out with a Cary 5000 UV/Vis/NIR-spectrometer (Varian). Steady-state fluorescence emission measurements were performed with a FluoroMax®-3. Time-correlated single-photon counting and near-infrared steady state emission spectroscopy was performed with a FluoroLog®-3 spectro-fluorometer (Horiba). All spectra were corrected for the instrument response. Transmission electron microscopy was performed with a TEM 912 Omega (Zeiss). Femtosecond transient absorption studies were carried out using a Helios transient absorption pump/probe system from Ultrafast Systems with laser pulses feed by a CPA-2101 from Clark-MXR Inc. Raman spectra were recorded using a FT-Raman RFS 100 system from Bruker with a Ge detector using a 1064 nm using a Nd-YAG laser for excitation.

Computational model systems were built based on a 100 ps molecular dynamics run of a (7,5)-SWCNT/PVBTA system in aqueous solution, with 40 chloride counterions. This simulation was performed at ambient pressure and 300 K (NPT ensemble) using the COMPASS force field, as implemented in Forcite Plus.[37] The simulation box was sized 90×94×85 $Å^3$ with periodic boundary conditions in all three dimensions. The pCND model was based on our previous work.[37] To obtain a

negatively charged dot, eight amide groups were replaced by carboxylates.

The molecular electrostatic potential was calculated with EMPIRE, using the semiempirical AM1 Hamiltonian and 1D periodic boundary conditions along the tube axis.[38,39] The Figures were made with VMD.[40]

Acknowledgements

The acknowledgements come at the end of an article after the conclusions and before the notes and references. This work was supported by the Deutsche Forschungsgemeinschaft as part of Collaborative Research Centre SFB 953 "Synthetic Carbon Allotropes" and of the Excellence Cluster "Engineering of Advanced Materials". The Bayerische Staatsregierung is acknowledged for funding granted as part of the "Solar Technologies go Hybrid" initiative. Johannes T. Margraf is supported by a Beilstein Foundation Scholarship. Volker Strauss is supported by the "Universität Bayern e.V."

Notes and references

[a] Friedrich-Alexander-Universität Erlangen-Nürnberg, Department of Chemistry and Pharmacy & Interdisciplinary Center for Molecular Materials (ICMM), Egerlandstrasse 3, 91058 Erlangen, Germany. E-mail: dirk.guldi@fau.de; Fax: +49-9131-852-8307

[b] Computer-Chemie-Centrum & Interdisciplinary Center for Molecular Materials (ICMM), Friedrich-Alexander-Universität Erlangen-Nürnberg, Nägelsbachstr. 25, 91058 Erlangen, Germany

1 V. Sgobba and D. M. Guldi, *Chem. Soc. Rev.*, 2009, **38**, 165.

2 M. H. Al-Saleh and U. Sundararaj, *Composites Part A*, 2011, **42**, 2126.

3 Y. Hou, J. Tang, H. Zhang, C. Qian, Y. Feng, and J. Liu, *ACS Nano*, 2009, **3**, 1057.

4 J. Li, X. Cheng, J. Sun, C. Brand, A. Shashurin, M. Reeves, and M. Keidar, *J. Appl. Phys.*, 2014, **115**, 164301.

5 D. Jariwala, V. K. Sangwan, L. J. Lauhon, T. J. Marks, and M. C. Hersam, *Chem. Soc. Rev.*, 2013, **42**, 2824.

6 J. P. Paraknowitsch and A. Thomas, *Energy Environ. Sci.*, 2013, **6**, 2839.

7 H. Li, Z. Kang, Y. Liu, and S.-T. Lee, *J. Mater. Chem.*, 2012, **22**, 24230.

8 L. Chen, Y. Hernandez, X. Feng, and K. Müllen, *Angew. Chem.*, 2012, **51**, 7640.

9 H. Wang, T. Maiyalagan, and X. Wang, *ACS Catalysis*, 2012, **2**, 781.

10 R. D. Costa, S. Feihl, A. Kahnt, S. Gambhir, D. L. Officer, G. G. Wallace, M. I. Lucio, M. A. Herrero, E. Vázquez, Z. Syrgiannis, M. Prato, and D. M. Guldi, *Adv. Mater.*, 2013, **25**, 6513.

11 N. Komatsu and F. Wang, *Materials*, 2010, **3**, 3818.

12 Y. Y. Huang and E. M. Terentjev, *Polymers*, 2012, **4**, 275.

13 C. Soulié-Ziakovic, R. Nicolaÿ, A. Prevoteau, and L. Leibler, *Chemistry*, 2014, **20**, 1210.

14 C. Romero-Nieto, R. García, M. Á. Herranz, L. Rodríguez-Pérez, M. Sánchez-Navarro, J. Rojo, N. Martín, and D. M. Guldi, *Angew. Chem. Int. Ed. Engl.*, 2013, **52**, 10216.

15 C. Romero-Nieto, R. García, M. Á. Herranz, C. Ehli, M. Ruppert, A. Hirsch, D. M. Guldi, and N. Martín, *J. Am. Chem. Soc.*, 2012, **134**, 9183.

16 V. Strauß, A. Gallego, G. de la Torre, T. W. Chamberlain, A. N. Khlobystov, T. T. Torres, and D. M. Guldi, *Faraday Discuss.*, 2014, **172**, 61.

17 F. D'Souza and O. Ito, *Chem. Commun*, 2009, 4913.

18 C. Backes, F. Hauke, C. D. Schmidt, and A. Hirsch, *Chem. Commun.*, 2009, **7345**, 2643.

19 B. B. Parekh, G. Fanchini, G. Eda, and M. Chhowalla, *Appl. Phys. Lett.*, 2007, **90**, 121913.

20 D. A. Britz and A. N. Khlobystov, *Chem. Soc. Rev.*, 2006, **35**, 637.

21 M. Ince, A. Hausmann, M. V. Martínez-Díaz, D. M. Guldi, and T. Torres, *Chem. Commun.*, 2012, **48**, 4058.

22 C. Backes, F. Hauke, and A. Hirsch, *Adv. Mater.*, 2011, **23**, 2588.

23 J. Bartelmess, A. R. M. Soares, M. V. Martínez-Díaz, M. G. P. M. S. Neves, A. C. Tomé, J. A. S. J. A. S. Cavaleiro, T. T. Torres, D. M. Guldi, M. V. Martinez-Diaz, and A. C. Tome, *Chem. Commun.*, 2011, **47**, 3490.

24 A. S. D. Sandanayaka, N. K. Subbaiyan, S. K. Das, R. Chitta, E. Maligaspe, T. Hasobe, O. Ito, and F. D'Souza, *ChemPhysChem*, 2011, **12**, 2266.

25 C. Oelsner, C. Schmidt, F. Hauke, M. Prato, A. Hirsch, and D. M. Guldi, *J. Am. Chem. Soc.*, 2011, **133**, 4580.

26 T. Hasobe, S. Fukuzumi, and P. V Kamat, *J. Phys. Chem. B.*, 2006, **110**, 25477.

27 M. Ohtani and S. Fukuzumi, *Chem. Commun.*, 2009, 4997.

28 V. Strauss, J. T. Margraf, C. Dolle, B. Butz, T. J. Nacken, J. Walter, W. Bauer, W. Peukert, E. Spiecker, T. Clark, and D. M. Guldi, *J. Am. Chem. Soc.*, 2014, **136**, 17308.

29 X. Wang, N. Behabtu, C. C. Young, D. E. Tsentalovich, M. Pasquali, J. Kono, *Adv. Funct. Mater.* 2014, **24**, 3241.

30 G. M. A. Rahman, A. Troeger, V. Sgobba, D. M. Guldi, N. Jux, M. N. Tchoul, W. T. Ford, A. Mateo-Alonso, M. Prato, *Chem. - A Eur. J.* 2008, **14**, 8837.

31 S. Leubner, G. Katsukis, D. M. Guldi, *Faraday Discuss.* 2012, **155**, 253.

32 R. D. Silvy, Y. Tan, P. Wallis, *Single-walled Carbon Nanotubes: Recent Advances, Manufacturing, Characterization and Applications, http://www.sigmaaldrich.com*, January 22nd, 2015

33 *http://www.nanointegris.com/en/hipco*, January 22nd, 2015.

34 M. J. O. Connell, S. M. Bachilo, C. B. Huffman, K. L. Rialon, P. J. Boul, W. H. Noon, M. J. O'Connell, V. C. Moore, M. S. Strano, E. H. Haroz, C. Kittrell, J. Ma, R. H. Hauge, R. B. Weisman, and R. E. Smalley, *Science*, 2002, **297**, 593.

35 A. G. Souza Filho, A. Jorio, G. G. Samsonidze, G. Dresselhaus, R. Saito, M. S. Dresselhaus, *Nanotechnology*, 2003, **14**, 1130.

36 Comprehensive studies on the spectroscopic properties of the reduced and oxidized species of pCNDs are in progress.

37 H. Sun, *J. Phys. Chem. B*, 1998, **102**, 7338.

38 M. Hennemann and T. Clark, *J. Mol. Model.*, 2014, **20**, 2331.

39 M. J. S. Dewar, E. G. Zoebisch, E. F. Healy, and J. J. P. Stewart, *J. Am. Chem. Soc.*, 1985, **107**, 3902.

40 W. Humphrey, A. Dalke, and K. Schulten, *J. Molec. Graphics*, 1996, **14**, 33.